



Comparison of airborne in situ measurements and Moderate Resolution Imaging Spectroradiometer (MODIS) retrievals of cirrus cloud optical and microphysical properties during the Midlatitude Cirrus Experiment (MidCiX)

Sean M. Davis,^{1,2} Linnea M. Avallone,¹ Brian H. Kahn,^{3,4} Kerry G. Meyer,⁵ and Darrel Baumgardner⁶

Received 17 April 2008; revised 9 October 2008; accepted 30 October 2008; published 22 January 2009.

[1] During the Midlatitude Cirrus Experiment (MidCiX), in situ measurements of cirrus cloud microphysical properties were made from aboard the NASA WB-57F aircraft in conjunction with Terra and Aqua satellite overpasses. These in situ data are directly compared to retrievals of cirrus visible optical thickness (τ), effective size (D_e), and ice water path (IWP) from the Moderate Resolution Imaging Spectroradiometer (MODIS) instruments aboard Terra and Aqua. The MODIS data considered here include both the operational retrieval (MOD06) and visible optical thickness retrieved from the 1.38- μm channel. Instruments aboard the WB-57F included three bulk probes for measuring ice water content (IWC), a cloud integrating nephelometer for measuring the visible extinction coefficient (β), and four optical particle probe instruments from which β and D_e are inferred. In situ β (IWC) data taken during vertical spiral profiles through cirrus are integrated to get τ (IWP) for comparison with MODIS values, and a methodology for comparing satellite and aircraft data is developed and illustrated using several case studies from MidCiX. It is found that the presence of cirrus overlapping low cloud layers significantly biases the MODIS operational τ to high values. For single-layer cirrus cases, the in situ IWP agree with MODIS values to within 20%, on average. The in situ τ/D_e differ from MODIS values in a manner that is roughly consistent with previous claims of particle shattering on aircraft inlets, although the magnitude of the differences is less than expected, and biases in the MODIS retrievals cannot be ruled out.

Citation: Davis, S. M., L. M. Avallone, B. H. Kahn, K. G. Meyer, and D. Baumgardner (2009), Comparison of airborne in situ measurements and Moderate Resolution Imaging Spectroradiometer (MODIS) retrievals of cirrus cloud optical and microphysical properties during the Midlatitude Cirrus Experiment (MidCiX), *J. Geophys. Res.*, 114, D02203, doi:10.1029/2008JD010284.

1. Introduction

[2] Ice clouds are ubiquitous in the Earth's atmosphere and play an important role in the radiation budget. Observations of cirrus microphysical properties from instruments on aircraft and passive satellite remote sensors are necessary for improving understanding of microphysical processes, and for monitoring and quantifying potential long-term changes in

cloudiness and cloud radiative effects. In general, airborne instruments are expected to provide the most accurate, spatially representative measurements of cloud microphysical properties at the highest temporal/spatial resolution, whereas passive satellite data provide information on the global distributions of vertically integrated cloud properties such as optical thickness (τ) and ice water path (IWP).

[3] In situ measurements of cirrus cloud microphysical properties from aircraft are relatively few in part because of the relative difficulty of reaching the upper troposphere. In addition, recent concerns over ice crystal shattering on aircraft and inlet surfaces have called into question the accuracy of these measurements. It has been hypothesized that ice crystal fragments from shattering events bias the particle probe and cloud integrating nephelometer (CIN) measurements from which extinction and effective particle size are inferred [e.g., *Heymsfield et al.*, 2006; *McFarquhar et al.*, 2007], although the significance of this effect has been contested [*Garrett*, 2007; *Gerber*, 2007].

[4] From the passive satellite remote sensing perspective, cirrus clouds are semitransparent in visible/IR channels and are

¹Laboratory for Atmospheric and Space Physics, University of Colorado, Boulder, Colorado, USA.

²Now at Cooperative Institute for Research in Environmental Sciences, University of Colorado, Boulder, Colorado, USA.

³Joint Institute for Regional Earth System Science and Engineering, University of California, Los Angeles, California, USA.

⁴NASA Jet Propulsion Laboratory, California Institute of Technology, Pasadena, California, USA.

⁵NASA Goddard Space Flight Center, Greenbelt, Maryland, USA.

⁶Centro de Ciencias de la Atmosfera, Universidad Nacional Autonoma de Mexico, Mexico City, Mexico.

difficult to measure with high precision because of their weak radiative signatures. Within the context of these measurement challenges, relatively little work has been done to assess the agreement between satellite-based microphysical property retrievals and in situ measurements from aircraft. Furthermore, the methodology for making meaningful comparisons between satellite and aircraft measurements is not well established for quantities that are known to possess strong spatial and temporal variations. In this paper, cirrus cloud visible optical thickness (τ), ice water path (IWP), and effective diameter (D_e) data from aircraft and satellite measurements with temporal and spatial coincidence are compared. These comparisons are assessed within the context of measurement uncertainty and the limitations associated with comparison of observations obtained by two very different types of sampling.

[5] This work builds on previous efforts to compare satellite-derived cloud properties with ground or aircraft measurements, but is one of only a few studies to date that have compared aircraft in situ data directly to satellite passive remote sensing of cirrus microphysical and optical properties [e.g., *Wielicki et al.*, 1990]. In fact, for cirrus optical/microphysical property observations, there have also been relatively few comparisons of satellite data with either ground-based data [*Chiriaco et al.*, 2007; *Elouragini et al.*, 2005; *Mace et al.*, 2005; *Yue et al.*, 2007] or satellite versus aircraft-based remote sensor data [*Chiriaco et al.*, 2007; *Rolland et al.*, 2000]. On the other hand, numerous studies have intercompared cloud top height or pressure measured from satellite and ground-based platforms [*Chang and Li*, 2005b; *Hawkinson et al.*, 2005; *Hollars et al.*, 2004; *Kahn et al.*, 2007; *Naud et al.*, 2004; *Naud et al.*, 2007; *Smith and Platt*, 1978; *Vanbaucce et al.*, 2003], from satellite and aircraft platforms [*Sherwood et al.*, 2004], and among satellite platforms [*Mahesh et al.*, 2004; *Naud et al.*, 2002; *Stubenrauch et al.*, 2005; *Wylie and Wang*, 1999].

[6] In this paper, in situ cirrus data from the NASA WB-57F aircraft taken during the Midlatitude Cirrus Experiment (Mid-CiX) in 2004 are compared with data taken contemporaneously by the Moderate Resolution Imaging Spectroradiometer (MODIS) instrument. During MidCiX, WB-57F flight patterns were coordinated with overpasses of the Terra and Aqua satellite platforms that carry the MODIS instruments. Because of the extensive cloud-physics payload that flew aboard the WB-57F and the direct coordination between the aircraft and Terra/Aqua overpasses, MidCiX data provide a unique opportunity for intercomparing these measurements.

[7] Section 2 presents a brief overview of the aircraft and satellite instruments, cirrus observations and retrievals, and methods for intercomparison. Then, individual case studies of coincident data from MidCiX are presented and used to explain the methodology and highlight the challenges inherent in aircraft-satellite comparisons. Finally, data from these case studies and other MidCiX flights are combined and used to evaluate the overall level of agreement between the MODIS and in situ measurements, and to address potential biases due to cloud overlap and particle shattering on aircraft and inlet surfaces.

2. Instruments and Methods

2.1. MODIS Cirrus Retrievals

[8] The satellite data used in this study come from the Moderate Resolution Imaging Spectroradiometer (MODIS)

instruments aboard the NASA Terra and Aqua satellites. MODIS measures in 36 wavelength bands spanning the visible to infrared (0.4–14.4 μm) [*King et al.*, 1997] with a horizontal resolution of 250 m to 1 km (depending on the channel) and a 55 degree field-of-view, yielding a swath width of approximately 2330 km in the cross-track direction. Here, we use the MODIS Collection 5 MOD06/MYD06 Level 2 cloud products [*Platnick et al.*, 2003] (see also M. D. King et al., Collection 005 Change Summary for the MODIS Cloud Optical Property (06_OD) Algorithm, 2006, http://modis-atmos.gsfc.nasa.gov/C005_Changes/C005_CloudOpticalProperties_ver311.p) (hereinafter referred to as King et al. online algorithm, 2006) that include retrievals (under daytime/sunlit conditions) of visible optical thickness (τ), effective radius (r_e), cloud water path (calculated from τ and r_e), and thermodynamic phase and multilayer information, among many others. Also included in the Collection 5 version of the MODIS data are uncertainty estimates for τ , r_e , and cloud water path (King et al., online algorithm, 2006).

[9] There are several limitations of the MODIS cloud optical property retrieval that significantly impact the comparisons shown later in this paper. First, the radiative transfer forward model in the operational retrieval is designed for single-layer cloud cases. Overlapping cloud layers in the atmosphere are very common [e.g., *Chang and Li*, 2005a; *Tian and Curry*, 1989; *Wang and Dessler*, 2006; *Warren et al.*, 1985], and the interpretation of the retrieved optical properties as a simple sum or average of the properties of the individual cloud layers is not justified [*Chang and Li*, 2005b]. Because of this, the MODIS operational retrieval may not accurately describe the properties of these types of cloud scenes. Furthermore, each cloudy pixel is only classified as liquid or ice, even though it is very common for ice clouds to overlay liquid clouds, or for liquid and ice phases to coexist within the horizontal scale of a pixel [*Nasiri and Kahn*, 2008]. As the thermodynamic phase determines which look-up table is used for retrieving optical thickness and effective radius, optical property retrievals for pixels with multilayered or mixed-phase clouds have the potential to be further biased on the basis of their retrieved thermodynamic phase.

[10] Another limitation of the MODIS operational optical property retrieval is that it is likely to fail in cases of “thin cirrus.” The theory upon which the MODIS retrieval is based was developed for optically thick clouds ($\tau \sim 7$) [*Nakajima and King*, 1990], but values returned by the MODIS retrieval extend to much thinner clouds ($\tau < 1$). Previous work indicates that pixels identified by MODIS as “cloudy” have $\tau \geq 0.2$ – 0.3 [*Dessler and Yang*, 2003], which represents an approximate lower limit to the MODIS operational τ .

[11] Because of the limitations of the operational retrieval with respect to thin cirrus and contamination from lower cloud layers, a new complementary algorithm has been devised to retrieve cirrus optical thickness (hereafter $\tau_{1.38}$) using reflectances from the 0.66- and 1.38- μm channels [*Meyer et al.*, 2007]. The unique 1.38- μm “cirrus” channel aboard MODIS is sensitive to scattering from ice crystals, but is dominated by absorption of water vapor in the lower atmosphere, making it ideal for separating high ice clouds from underlying water clouds and the land surface [*Gao and*

Kaufman, 1995]. Because the 1.38- μm retrieval is slightly sensitive to the assumed effective size (approximately 1% change in optical thickness per μm change in the assumed D_e) [*Meyer et al.*, 2007], we use the operationally retrieved effective size, when available.

2.2. In Situ Measurements

[12] The MidCiX campaign was based at Ellington Field in Houston, Texas, during April and May of 2004. MidCiX consisted of nine flights, with seven coincident overpasses total between Aqua and Terra. The clouds sampled during the overpasses included both in situ and convectively generated cirrus.

[13] Three “bulk” instruments that measure total water (from which ice water content can be calculated) flew on the NASA WB-57F during MidCiX: the University of Colorado closed-path laser hygrometer (CLH) [*Davis et al.*, 2007b], the Droplet Measurement Technologies Cloud Spectrometer and Impactor (CSI) [*Twohy et al.*, 1997], and the Harvard University Lyman- α photofragment fluorescence total water hygrometer (HT) [*Weinstock et al.*, 2006b, 2006a]. Ice water content data from these instruments are reported at 1 Hz, and generally agree within the stated instrumental uncertainties [*Davis et al.*, 2007a].

[14] Several optical particle probe instruments were flown during MidCiX. Data from these probes are used to calculate the visible extinction coefficient (β , km^{-1}) and effective diameter (D_e , μm) within cloud (see section 2.3) at 10-s intervals along the flight track. The Cloud Aerosol and Precipitation Spectrometer (CAPS) measures particles ranging in dimension from 0.5 to $\sim 1500 \mu\text{m}$ [*Baumgardner et al.*, 2001]. CAPS consists of two probes: the Cloud and Aerosol Spectrometer (CAS), measuring particles from 0.5 to $50 \mu\text{m}$, and the Cloud Imaging Probe (CIP), which images particles from 25 to $1600 \mu\text{m}$. During MidCiX, a flow-straightening shroud was present over the CAS inlet. It has been hypothesized that the shroud causes ice crystals to shatter, thereby contaminating the CAS measurement [*McFarquhar et al.*, 2007]. The effects of shattering in the CAS data are corrected for by scaling the CAS data on the basis of an automated comparison of the CAS and CIP data in the overlap region between 25 and $50 \mu\text{m}$ (*D. Baumgardner et al.*, manuscript in preparation, 2008).

[15] The Cloud Particle Imager (CPI) [*Lawson et al.*, 2001] measures the PSD from ~ 5 to $1000 \mu\text{m}$ on the basis of imagery (number per size bin) that is scaled using the total particle concentration (L^{-1}) obtained from an integrated particle detection system. Because of large uncertainties in the sampling efficiency for small particles (*P. Lawson*, personal communication, 2008), data from the SPP-100 are substituted for particles smaller than $47 \mu\text{m}$. The SPP-100 probe is a repackaged Forward Scattering Spectrometer Probe (FSSP-100) that uses a measurement principle similar to that of the CAS and measures sizes from 0.9 to $47 \mu\text{m}$.

[16] In addition to the particle probes, the visible extinction coefficient (β) was measured by the Cloud Integrating Nephelometer (CIN) [*Gerber et al.*, 2000]. CIN uses four sensors spanning angles from 10° to 175° to measure the intensity of light scattered by particles passing through the beam path of a 635-nm wavelength laser. The angular dependence of the scattered light is used to calculate the asymmetry parameter (g) and the extinction coefficient (β).

Data are recorded at 5 Hz, and reported as a 9-s running mean at 1 Hz. These data are used at 10-s intervals to be consistent with the optical particle probe data.

[17] Finally, meteorological and aircraft position measurements used here are from the Meteorological Measurement System (MMS) [*Scott et al.*, 1990]. The MMS provides measurements of the ambient pressure ($\pm 0.25 \text{ hPa}$ accuracy), temperature ($\pm 0.25 \text{ K}$), aircraft true air speed ($\pm 1 \text{ m s}^{-1}$), horizontal and vertical wind speeds ($\pm 1 \text{ m s}^{-1}$), and GPS location (latitude, longitude, altitude).

2.3. Optical Thickness, Ice Water Path, and Effective Size Determination Using In Situ Data

[18] From Mie theory, the extinction coefficient for a given particle at a specific wavelength is the particle’s cross-sectional area multiplied by the extinction efficiency. For cirrus particles (greater than a few microns in diameter) at a commonly used reference wavelength of 650 nm, the extinction efficiency is 2, because the Mie size parameter is in the geometric optics limit (i.e., $2\pi r/\lambda \gg 10$). The extinction coefficient of an ensemble of cirrus particles at this visible wavelength (β , km^{-1}) is given by

$$\beta = 2 \int A(D) dD, \quad (1)$$

where $A(D)$ is the cross-sectional (projected) area density ($\mu\text{m}^2 \mu\text{m}^{-4}$) of particles with dimension D . Here, $A(D)$ is estimated from the SPP, CPI (+SPP), and CAPS data and used to calculate β . From CIP and CPI data, $A(D)$ is computed directly from the particle image data. Particles smaller than $50 \mu\text{m}$ (i.e., those measured by CAS and SPP-100) are assumed to be spherical for the purposes of calculating $A(D)$. This is a common assumption [e.g., *Heymsfield et al.*, 2006] and is qualitatively confirmed by CPI imagery during MidCiX.

[19] From these various estimates of β , it is possible to calculate the optical thickness of a cirrus layer that is sampled in a spiral “corkscrew” pattern by the WB-57F, using

$$\tau = \sum_{i_{\text{bottom}}}^{i_{\text{top}}} \beta_i \Delta z_i, \quad (2)$$

where β_i are the in situ extinction measurements (from CIN or the particle instruments) and Δz_i are the changes in altitude between each pair of data points. Similarly, ice water path (IWP) is calculated using

$$IWP = \sum_{i_{\text{bottom}}}^{i_{\text{top}}} W_i \Delta z_i, \quad (3)$$

where W_i are the IWC measurements. These methods for calculating τ and IWP assume that the spiral performed by the WB-57F suitably approximates a “vertical” profile. This issue is addressed in section 3.

[20] The effective diameter is also calculated from both the CIN and particle probe data for comparison to the MODIS retrievals, using

$$D_e = \frac{3W}{\rho_{\text{ice}}\beta}, \quad (4)$$

where ρ_{ice} is the bulk density of ice (0.93 g cm^{-3}), W is in units of mg m^{-3} , and β is in units of km^{-1} [Mitchell, 2002]. For calculating D_e using the CIN β , IWC data from the CLH instrument are used. For the particle probes, β is calculated as in equation (1). For particles measured by CAS and SPP-100, spheres are assumed for calculating the contribution to W from particles smaller than $50 \mu\text{m}$. For the CPI and CIP, W is calculated using the mass-dimensional relationships developed by Baker and Lawson [2006]. These relationships relate particle mass to either projected area (used for CIP data) or a combined size parameter (a combination of area, length, width, and perimeter, used for CPI data), and were shown by Baker and Lawson to give similar results in computing IWC for the data set they considered.

3. Case Studies

[21] During MidCiX, there were six sets of “corkscrew” spiral profiles through cirrus clouds that were performed in conjunction with Terra and Aqua overpasses. Most of these maneuvers involved a downward spiral (with horizontal diameter on the order of 10 km), followed by an upward spiral through the same cloud region. In this section, two case studies are presented to illustrate the methodology that was developed to compare aircraft and satellite data. These case studies are also used to highlight the salient features of the satellite and aircraft data sets and IWP/ τ / D_e intercomparisons.

3.1. Case Study 1: 6 May 2004 Thin Cirrus Encounter

[22] During the 6 May 2004 MidCiX flight, the WB-57F performed a 6-min-long down-and-up spiral maneuver in thin cirrus over the Gulf of Mexico, near the coast of Louisiana. These clouds were associated with moist southwesterly flow on the eastern side of a closed upper-level low, and were prognosticated to move east, with stable or slightly increasing coverage throughout the time period of the flight. The spiral maneuver lasted from 1853 to 1859 UT, ending approximately 15 min before the Aqua overpass, which occurred at 1916 UT.

[23] To account for the movement of clouds between the time of aircraft sampling and satellite overpass, the WB-57F flight track is “advected” forward from the time of the aircraft measurements to the time of the satellite overpass using MMS-measured horizontal winds, latitudes, and longitudes at 1-s intervals during the spirals. The advected latitude (θ') and longitude (ϕ') for each MMS measurement of the u (E-W) and v (N-S) horizontal wind speeds, latitude (θ), and longitude (ϕ) are given by

$$\theta' = \theta + \frac{vt}{R} * \frac{180}{\pi} \quad (5)$$

$$\phi' = \phi + \frac{ut}{R \cos \theta} * \frac{180}{\pi}, \quad (6)$$

where R is the radius of the Earth at latitude θ and t is the time lag between the satellite and in situ data. For this spiral, the mean (± 1 standard deviation) values of u and v were $17 \pm 1.6 \text{ m s}^{-1}$ and $7 \pm 1.7 \text{ m s}^{-1}$, respectively. Using equations (5) and (6), the cloud moved about 20 km to the

NE between sampling by the aircraft and observation by satellite (Figure 1).

[24] The locations of the original and advected flight tracks are shown in Figure 1, overlaid on $\tau_{1.38}$ imagery. Because the cloud sampling occurred before the satellite overpass in this example, a contrail that was produced by the WB-57F is evident in this image. While the presence of a contrail is problematic for the satellite and in situ data intercomparison described below, it helps to illustrate the need for the advection scheme described above.

[25] Ideally, the advected flight track should overlay the contrail in the $\tau_{1.38}$ imagery. However, the advected flight track is offset WSW of the contrail by $\sim 5 \text{ km}$, even though the track has deformed in a way that matches the shape of the contrail seen in the MODIS imagery. Possible reasons for this offset include an underestimation of the horizontal wind speeds of $\sim 3\text{--}4 \text{ m s}^{-1}$, or a divergence of the horizontal wind field. As the stated accuracy of the MMS horizontal winds is $\pm 1 \text{ m s}^{-1}$, we speculate that it is the heterogeneity of the wind field, and not the MMS measurements, that caused the offset between the advected track and the contrail.

[26] Independent of the slight mismatch between the advected flight track and contrail in Figure 1, it is clear that it would be misleading to compare the in situ data to the $\tau_{1.38}$ values within the nonadvected spiral region (orange box in Figure 1). Furthermore, the advected flight track does not overlay the isolated cloud region seen in the $\tau_{1.38}$ imagery, and thus the region around the advected spiral is the most appropriate for comparison with in situ data. Because a simple latitude/longitude bounding box (purple) includes a significant number of clear air pixels that have the potential to skew statistics derived from this region, the advected flight track is used as a guide and pixels that lie within the cloud region are manually chosen (blue bounding box) to avoid including clear air regions in the comparison.

[27] Figure 1 shows images of $\tau_{1.38}$ and the MODIS cloud-phase retrieval along with the actual and advected flight tracks. This plot reveals the failure of the MODIS operational algorithm to detect the thin cirrus layer sampled by the WB-57F. Most of the region in the vicinity of the contrail/cirrus feature is tagged as “No retrieval,” meaning that the pixels failed the decision tree test and no retrieval of τ or r_e was attempted. The plot also showcases the sensitivity of the $1.38\text{-}\mu\text{m}$ retrieval to thin cirrus and contrails, which are readily apparent in the image.

[28] Vertical profiles of IWC and β measured by the aircraft instruments during the spiral are also shown in Figure 1. Using equation (3), the IWPs of the downward and upward legs of the spiral from CLH (HT) are calculated to be 1.7 ± 0.04 (1.4 ± 0.9) and 2.5 ± 0.06 (1.8 ± 0.8) g m^{-2} , respectively. Here the IWP error is calculated by propagating the IWC uncertainty estimates at each 1-s data point through equation (3). The IWPs from this spiral do not agree as well as they do for some of the other passes, but are still within 50% of one another. This agreement is within the instrumental uncertainties given above, which were relatively high for this cloud encounter because of the small total water/water vapor contrast (i.e., a few ppm of ice on a background of ~ 100 ppm of vapor) on which these instruments rely. CSI data are not included in this analysis

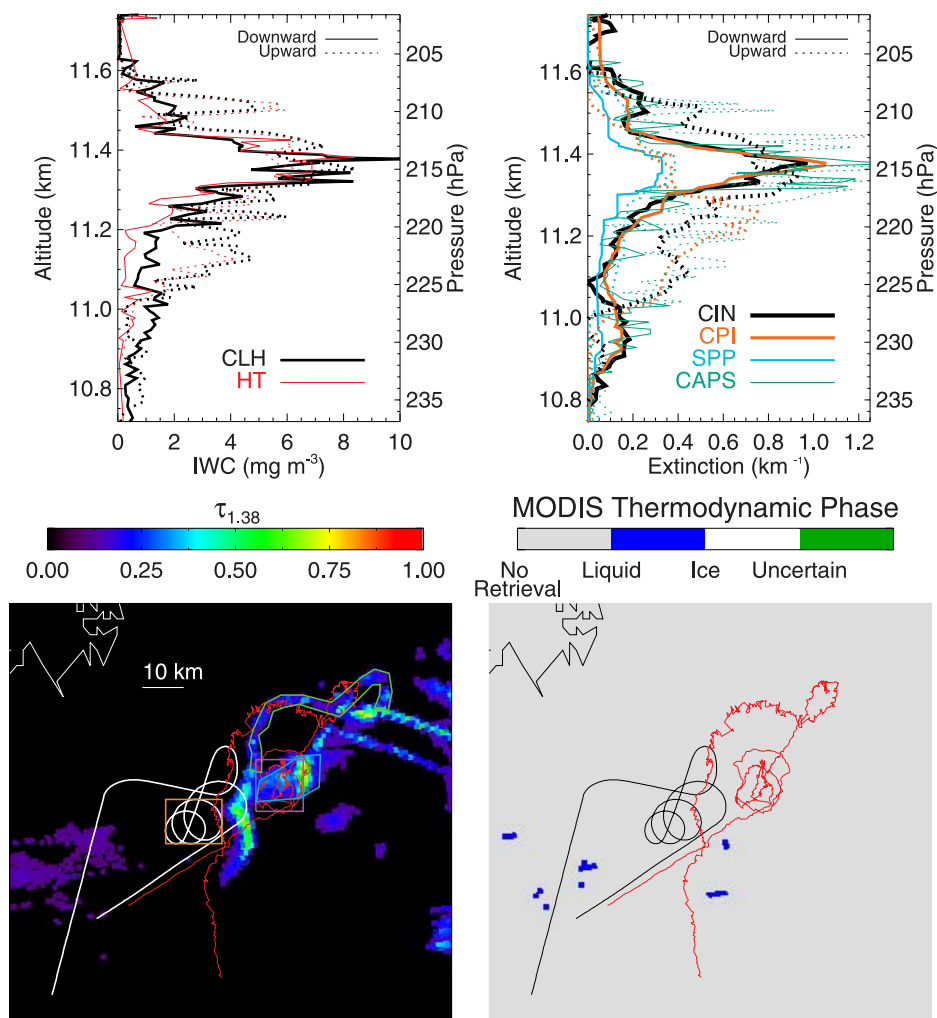


Figure 1. (top) Vertical profiles of IWC and β from the spirals, taken 1853–1859 UT during the 6 May 2004 MidCiX flight. (bottom) Images of the MODIS 1.38- μm optical thickness retrieval and operational thermodynamic phase retrieval. The white (black) line on the left (right) panel is the WB-57F flight track, and the red lines are the advected flight tracks.

because the instrument was not functioning during the 6 May flight.

[29] Vertical profiles of extinction for the 6 May flight are shown alongside the IWC profiles in Figure 1. The values of τ for the spirals are in the range ~ 0.1 – 0.3 , with SPP and CAPS giving the smallest and largest values, respectively. The mean effective diameters are $45 \mu\text{m}$ for CPI, $28 \mu\text{m}$ for CIN/CLH, $22 \mu\text{m}$ for CIN/HT, and $37 \mu\text{m}$ for CAPS.

[30] Figure 2 shows τ , IWP, and D_e data from the MODIS 1.38- μm retrieval, as well as the values calculated from the in situ measurements. Figure 2 (top) contains two histograms of $\tau_{1.38}$ (i.e., τ from the MODIS 1.38- μm retrieval): the blue histogram is composed of MODIS pixels within the manually chosen region corresponding to the cirrus sampled by the WB-57F (i.e., the blue region in Figure 1); the green histogram represents MODIS pixels within the contrail (i.e., the green region in Figure 1). Above these histograms are two horizontal bars (labeled $\tau_{1.38}$ and τ_{contrail}) representing the standard deviation ($\pm 1\sigma$) of values, as well as the mean (crosses), and median (pluses). Finally, the in situ optical thicknesses (τ_{CIN} , τ_{CPI} , τ_{SPP} , and τ_{CAPS}) are shown as

triangles, with the direction representing whether they are from the up (up-pointing triangles) or down (down-pointing triangles) portion of the spiral.

[31] IWP data are plotted in a similar manner. Because MODIS operational D_e are nonexistent for this example, the in situ effective diameters are combined with $\tau_{1.38}$ to calculate the MODIS 1.38- μm IWP by

$$IWP = \frac{1}{3} \rho_{\text{ice}} D_e \tau. \quad (7)$$

Ice water paths calculated this way are henceforth subscripted with the τ and D_e used to calculate them. As an example, the array of ice water paths calculated using the $\tau_{1.38, < \text{CAPS} >}$ and the mean CAPS D_e would be $IWP_{1.38, < \text{CAPS} >}$. Ice water paths from the MODIS operational retrieval of optical thickness (τ_{op}) and effective size are denoted as $IWP_{\text{op,op}}$.

[32] There are several striking features about these plots that warrant discussion. First, there is a significant amount of heterogeneity present in the MODIS values as evidenced

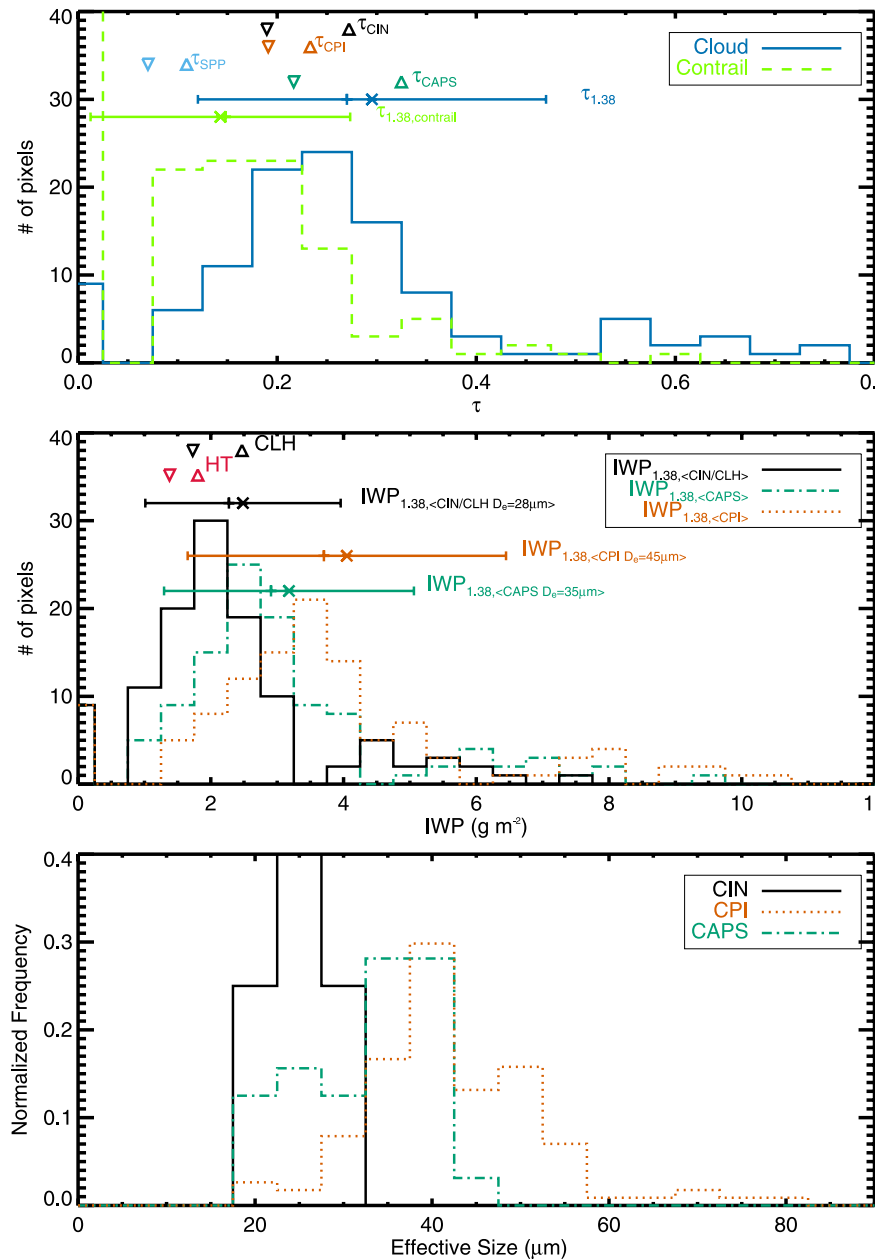


Figure 2. Histograms of τ , IWP, and D_e from the 6 May spiral. (top) The $\tau_{1.38}$ histograms over the cloud (blue) and contrail region (green). (middle) Histograms with IWP calculated from $\tau_{1.38}$ and the CAPS (green) or CIN (black) D_e . (bottom) Histograms of D_e . Downward (upward) pointing triangles denote τ or IWP from the in situ measurements for the downward (upward) spiral leg. The horizontal bars denote the standard deviation ($\pm 1\sigma$) of the $\tau_{1.38}$ and $\text{IWP}_{1.38}$ data, with the mean (median) values denoted by crosses (pluses).

by the width of the distributions of τ . There is also a significant spread among the values of τ from the different in situ measurements, as well as significant differences in τ between the downward and upward portions of the spiral. For every instrument, the optical thicknesses are larger in the upward leg by $\sim 50\text{--}100\%$. The consistency of this change from leg to leg among all instruments suggests that the differences from the downward to the upward spiral legs were real and related to microphysical heterogeneity along the WB-57F sampling path, and are not merely the result of instrument artifacts. This heterogeneity must also be con-

sidered in the context of horizontal variations in τ as observed by MODIS.

[33] Under idealized conditions such as cloud homogeneity (i.e., constant geometric thickness and randomly distributed microphysical properties), random particle orientation, and small spiral diameters (relative to the cloud horizontal size), one would expect that the “satellite-based” probability density functions (PDF) of τ from a nadir-looking instrument (e.g., MODIS) should be the same as the “aircraft” PDF of τ sampled from a sufficiently large number of independent spirals. In practice, cloud heteroge-

neity in the form of “roughness” (i.e., a nonflat vertical boundary), “patchiness” (i.e., clear air within the cloud), or gradients in microphysical properties, will cause the satellite and aircraft PDFs to differ. Also, particles tend to be oriented with their cross-sectional areas maximized normal to gravity, which has the potential to cause anisotropy in the extinction field if the particles are asymmetrical [e.g., *Chepfer et al.*, 1999]. This, as well as nonrandom orientation induced as particles flow around or through the aircraft and instrument surfaces, has the potential to render satellite and aircraft PDFs of τ different at a fundamental level.

[34] On a given day, it is not possible to compare the satellite and aircraft PDFs of τ and IWP in a statistically rigorous way because the in situ sample size is very limited (i.e., $N = 1$ or $N = 2$). In contrast, because D_e is a point quantity (as opposed to integrated quantities such as τ and IWP) that is measured continuously along the flight track, PDFs of D_e from the aircraft and MODIS can be compared in a statistical manner (e.g., see section 4), albeit with the same caveats concerning the fundamental comparability of the PDFs as discussed above.

[35] In Figure 2 (top), almost all of the in situ optical thicknesses fall within 1σ of the $\tau_{1.38}$ distribution, with τ_{SPP} being slightly lower than this range. Because the SPP does not measure the full range of particle sizes that contribute to extinction, it is not surprising that τ_{SPP} is on the low side. By including the extinction contribution from large particles, as measured by the CIP (i.e., $\tau_{SPP+CIP}$), the values are within 1σ of $\tau_{1.38}$ (not shown in Figure 2).

[36] The IWP data in Figure 2 (middle) are slightly more complicated than the optical thickness data. The in situ IWPs (triangles) are in good agreement with one another relative to their uncertainties, but there are again clear differences between the two spiral legs. The histograms of $IWP_{1.38,<CIN/CLH>}$ and $IWP_{1.38,<CPI>}$ span the range of values of D_e in the in situ data (28 μm from CIN and 45 μm from CPI). The median, mean, and range (standard deviation) of values of $IWP_{1.38,<CAPS>}$, $IWP_{1.38,<CPI>}$, and $IWP_{1.38,<CIN/CLH>}$ are plotted as horizontal bars as in Figure 2 (top). In this case, the median $IWP_{1.38,<CIN/CLH>}$ most closely matches the in situ IWPs, but the in situ IWPs are within the bounds of the $IWP_{1.38,<CPI>}$ histogram as well.

[37] However, the apparent agreement between the MODIS and in situ data in this case is likely spurious, as some of the observed $\tau_{1.38}$ is probably due to the WB-57F contrail. The onboard observer noted the presence of the contrail at 1857 UT during the upward leg of the spirals, and as illustrated by the histograms in Figure 1, the contrail optical thickness (median 0.15) is similar in magnitude to the cloud-region optical thickness (median 0.27). From this, it appears as though about half of the value of $\tau_{1.38}$ within the cloud region is due to the WB-57F contrail.

[38] It is worth noting that for two of the five other satellite/aircraft coincidences considered in this paper, aircraft data were taken after the satellite overpass. Of the remaining three, contrail production was noted in only one case (22 April), and it was in a significantly thicker cirrus cloud ($\tau \sim 2$). In this case, contrail production was observed only for a brief period near the cloud top, and the MODIS 1.38- μm imagery shows no sign of contrails in the vicinity of the cloud region. Assuming optical thicknesses on the

order of 0.1–0.25, which are typical for linear contrails [*Minnis et al.*, 2004], contrails do not affect any of the comparisons presented in this paper except for the 6 May case.

[39] The 6 May case described here illustrates the methodology developed for direct satellite/aircraft comparisons, although no definitive conclusions can be drawn about the agreement between the MODIS and in situ data due to contrail contamination. This case highlights the need to advect the flight track to correct for time lags between the satellite and aircraft comparisons, as well as the need for aircraft sampling to follow the satellite overpass in time when attempting to make meaningful comparisons in thin cirrus.

3.2. Case Study 2: 30 April 2004 Case Study in Thicker Cirrus

[40] During the 30 April 2004 MidCiX flight, the WB-57F sampled cirrus anvil blowoff near Tennessee that originated from a mesoscale convective system (MCS) located over southern Louisiana. Included in the sampling on this day was an 18-min-long Lagrangian spiral (1630–1648 UT), in which the plane drifted with the wind, which was coordinated with a Terra overpass at 1640 UT. A broad, low cloud deck was persistent throughout the spiral and subsequent cirrus sampling, as noted by the onboard observer.

[41] Figure 3 shows MODIS images in the vicinity of the spiral. In this scene, the MODIS operational algorithm identifies the pixels in the vicinity of the spiral as ice, and those in the surrounding region as liquid cloud. Although the color scales are different for the two τ images in Figure 3, it is clear that the MODIS 1.38- μm and operational values are quite different from one another. The $\tau_{1.38}$ is ~ 2 in the vicinity of the advected spiral track, whereas the τ_{op} is ~ 10 . In other parts of the image, the values can be different by more than an order of magnitude.

[42] The histograms of τ , IWP, and D_e in Figure 4, which are similar to those shown in Figure 2, clearly illustrate the disagreement between the MODIS retrievals. The values of τ estimated from the in situ measurements are in the range 0.8–3.3, with τ_{CPI} higher than $\tau_{1.38}$, and τ_{SPP} and τ_{CAPS} lower (there are no CIN data for this flight). Compared to the in situ τ and $\tau_{1.38}$, τ_{op} is approximately an order of magnitude larger, with a median value of 17.5.

[43] In terms of IWP, the MODIS operational retrieval is also about an order of magnitude larger than both the 1.38- μm retrieval and in situ data. The in situ values from the CLH, Harvard, and CSI instruments range from 13 to 18 g m^{-2} , which is significantly smaller than the mean value of 114 g m^{-2} from the operational retrieval. Because of the confidence in the accuracy of the in situ IWP [*Davis et al.*, 2007a], the three of which agree to within about 20% of one another, these data provide a fairly stringent constraint on the MODIS IWPs.

[44] Also, as Figure 4 illustrates, the values of $IWP_{1.38}$ calculated using the in situ D_e are in much closer agreement with the in situ IWP than the $IWP_{op,op}$. The best agreement with the in situ IWP is with $IWP_{1.38,op}$ (mean D_e of 22 μm). The CAPS D_e (36 μm) produces an IWP that is about a factor of 2 larger than the in situ IWP. This suggests either a high bias in the CAPS D_e or a high bias in $\tau_{1.38}$. Although

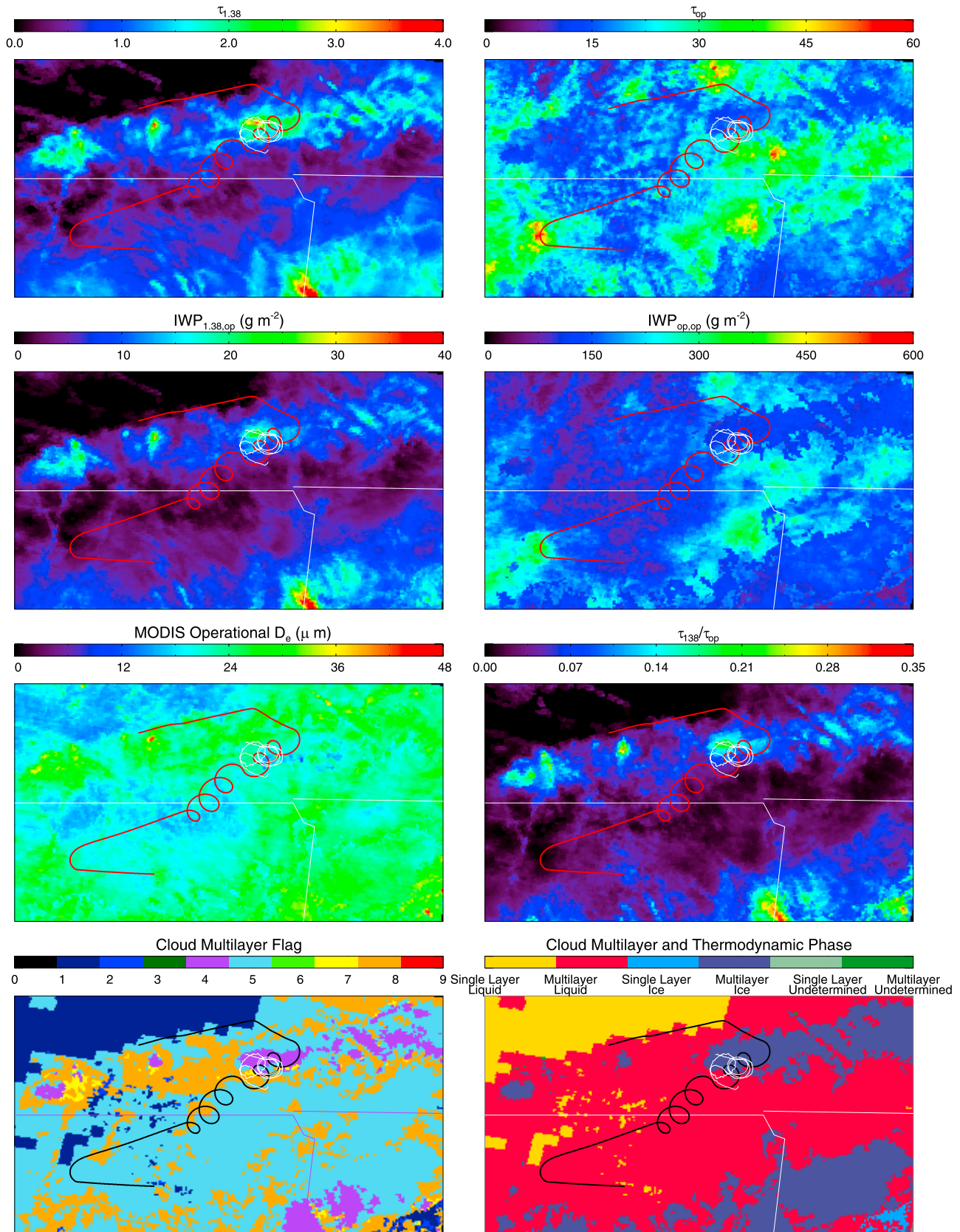


Figure 3. MODIS imagery during the 30 April MidCiX spiral with the WB-57F flight track overlaid. The advected flight track during the spiral is shown as a thin white line. The first row shows $\tau_{1.38}$ and τ_{op} ; the second row shows IWP; the third row illustrates (left) the operational D_e and (right) ratio of optical depth values; and the fourth row shows flags for multilayer clouds and cloud phase.

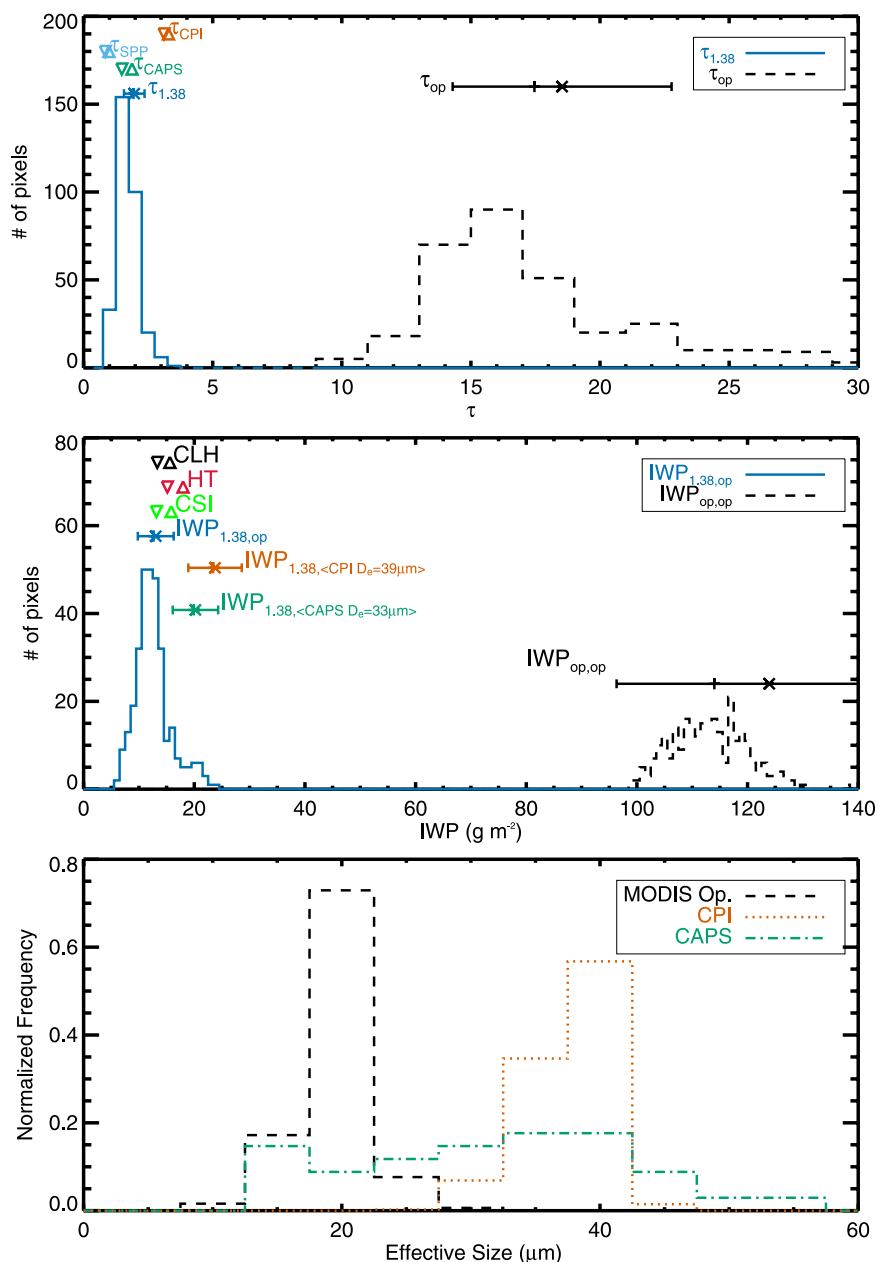


Figure 4. (top) Optical thickness, (middle) IWP, and (bottom) D_e histograms from the 30 April MidCiX spirals, similar to Figure 2. Triangles denote the in situ τ and IWP, and horizontal bars represent the standard deviation of MODIS-derived values.

$IWP_{1.38,op}$ is in agreement with the in situ data, it is possible that a high-biased $\tau_{1.38}$, and a low-biased MODIS D_e (see below) could explain this result.

[45] The most plausible reason for the large discrepancy between the operational retrieval and the in situ and 1.38- μm values is a radiative contribution from the lower liquid cloud layer, which was noted by the WB-57F onboard observer. Even though the thermodynamic phase algorithm correctly identifies the pixels in the vicinity of the spiral as being ice, the visible-band reflectance used to retrieve optical thickness presumably contains a large contribution from the lower cloud layer, which would tend to bias the τ_{op} to large values [e.g., King et al., 1997].

[46] In addition to the bias in τ_{op} caused by the low cloud layer, the MODIS D_e retrieval is likely biased toward a small value. A theoretical study by Platnick [2000] considered liquid clouds with specified vertical profiles of D_e , and used the concept of vertical weighting functions of reflectance to describe the location within cloud from which the measured MODIS reflectance originates. For the channels used for retrieving particle size in the MODIS retrieval, the weighting functions peak near an optical depth (i.e., the vertical coordinate into the cloud from the top) of unity, and contain significant contributions from altitudes below the $\tau = 1$ level. Judging by the 1.38- μm retrieval and the in situ measurements, the cirrus layer has an optical thickness of one or greater, so the operationally retrieved D_e probably

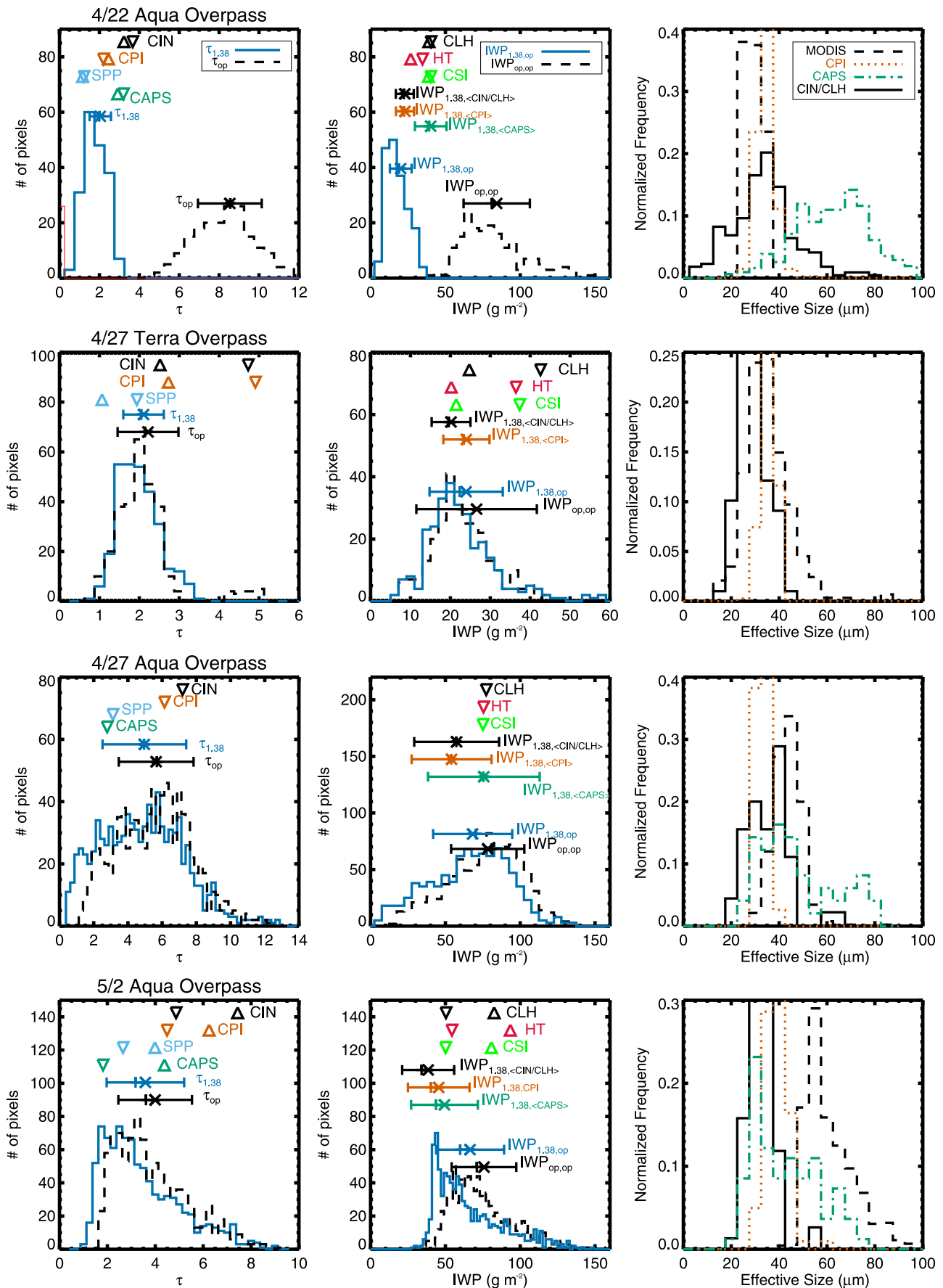


Figure 5

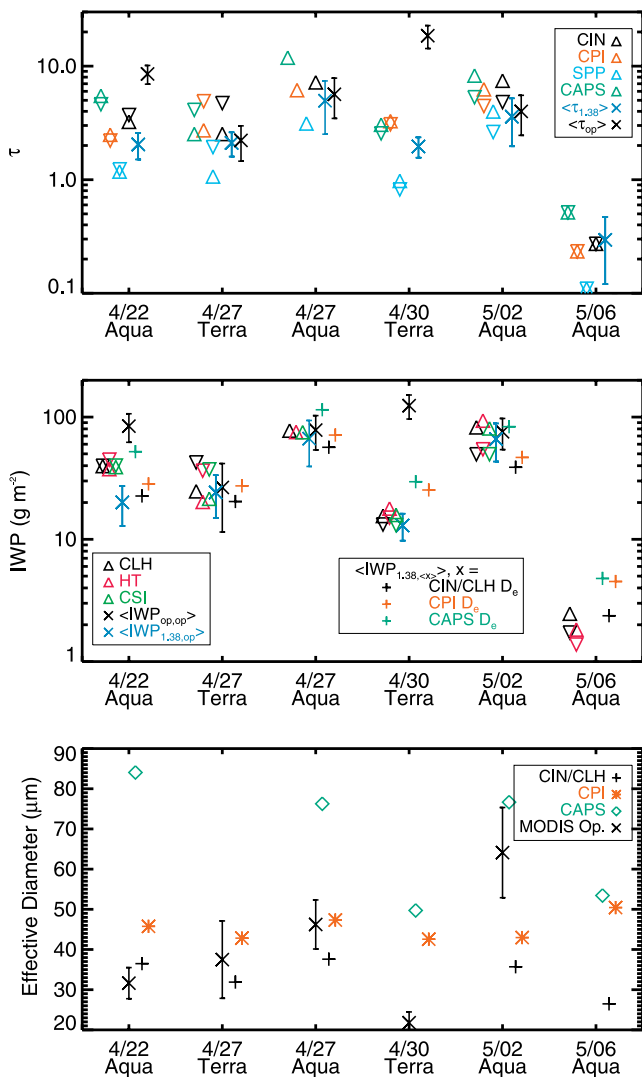


Figure 6. MODIS and in situ τ , IWP, and D_e from the MidCiX coincident overpasses. The color-coded triangles represent in situ data, with the direction of the triangles representing the direction of the spiral (up or down). X's represent the means of the two versions of the MODIS data. Vertical bars represent the standard deviation ($\pm 1\sigma$) of MODIS values within the cloud region. The color-coded pluses in the middle plot are the mean of the IWPs calculated using $\tau_{1.38}$ values and the mean in situ D_e from various instruments.

contains contributions from both the cirrus layer and the lower cloud layer. As liquid clouds typically contain smaller drop sizes than ice clouds, the presence of the lower layer would presumably bias the retrieved D_e toward smaller values. Indeed, the mean MODIS D_e in this case was $22 \mu\text{m}$, which is smaller than any of the in situ particle probes indicate.

[47] One issue raised by the implication that τ_{op} is strongly biased in the presence of cloud overlap is whether or not multilayered scenes can be properly identified on an operational basis. Figure 3 shows the results of a new algorithm for identifying pixels containing multiple cloud layers (“Cloud_Multi_Layer_Flag” in the collection 5 MOD06 data product) (King et al., online algorithm, 2006), as well as the multilayer and thermodynamic phase algorithms (“Quality_Assurance_1km,” in MOD06). In this example, the multilayer algorithm identifies pixels in the sampled cloud region as being multilayer with a high confidence level, and the thermodynamic phase algorithm identifies the pixels as ice. Thus, for this case study, the MODIS operational retrieval shows a promising ability to detect multilayered cloud scenes and provide information necessary to identify pixels in which the operational τ , IWP and D_e are potentially contaminated by low cloud layers.

4. Comparisons of MODIS and in Situ Data During MidCiX

[48] The case studies in the previous two sections were used to illustrate the methodology for comparing MODIS and in situ data, and to identify some of the preliminary results of the comparison. In this section, data from four additional overpasses that were coincident with WB-57F spirals are combined with the two case studies, and the overall comparison between MODIS and in situ data during MidCiX is presented. For brevity, the additional cases are not described in detail, but histograms of the optical/microphysical properties (similar to Figures 2 and 4) are shown in Figure 5, and all data are shown as a function of day in Figure 6. As with the case studies introduced in section 3, the cloud region on each day is manually defined using the advected flight track as a guide. Related to these plots, data for each of the MidCiX case studies are summarized in Table 1, and the results of statistical comparisons between the data sets are shown in Tables 2 and 3.

[49] Tables 2 and 3 give the percent differences between the in situ and MODIS data, and the results of Student's t test comparisons between the data sets. For IWP, τ , and D_e , the in situ values for each day are aggregated and compared to the mean values from MODIS. The comparisons have been grouped into single-layered cloud cases, multilayered cloud cases, or “all” cases to support the discussion below.

[50] These statistical comparisons provide a metric to assess whether the means of the distributions are statistically different from each other, relative to their standard errors. It is worth noting that these tests do not explicitly take into account measurement error, although both measurement error and atmospheric variability affect the width of the distributions, and hence the value of the standard error that goes into the calculation.

[51] The additional data shown in Figures 5 and 6 and Tables 1–3 support the preliminary analysis of the 30 April case, which indicated that the MODIS operational retrieval

Figure 5. MOD06 cloud multilayer and thermodynamic phase flags for the 30 April MidCiX case. The cloud multilayer flag ranges from 0 to 9, with 0 for clear air pixels, 1 for single-layered clouds, and 2–9 representing multilayer clouds, with the higher numbers indicating an increased confidence that the pixel is multilayered. Data from the 22 April, 27 April, and 2 May Terra/Aqua overpasses during MidCiX, similar to Figures 2 and 4.

Table 1. MidCiX Spiral Data

	Date (mddd)					
	0422	0427	0427	0430	0502	0506
MODIS Time, UT	1903	1920	1750	1642	1940	1916
Spiral Start Time, UT	1820	2013	1750	1630	1911	1853
Spiral End Time, UT	1910	2021	1755	1648	1926	1859
Pressure (hPa)	306	285	238	212	276	218
Temperature (K)	235	231	217	215	229	218
Base altitude (km)	7.6	8.5	9.4	10.5	8.6	10.7
Thickness (km)	3.0	2.2	2.8	2.5	2.6	1.1
Satellite	Aqua	Aqua	Terra	Terra	Aqua	Aqua
Surface	Ocean	Ocean	Land	Land	Ocean	Ocean
Low Cloud	Yes	No	No	Yes	No	No
N _{Hz}	3000	480	1200	1080	900	360
N _{Spiral}	2	1	2	2	2	2
N _{MODIS}	187	901	288	314	919	115
	Date (mddd)					
	0422	0427	0427	0430	0502	0506
	Mean ± 1σ or Min-Max ^a	Mean ± 1σ or Min-Max ^a	Mean ± 1σ or Min-Max ^a	Mean ± 1σ or Min-Max ^a	Mean ± 1σ or Min-Max ^a	Mean ± 1σ or Min-Max ^a
MODIS τ _{op}	8.5 ± 1.6	5.7 ± 2.2	2.3 ± 0.8	18.5 ± 4.2	4.0 ± 1.5	-
MODIS τ _{1.38}	2.0 ± 0.5	5.0 ± 2.4	2.1 ± 0.5	2.0 ± 0.4	3.6 ± 1.6	0.30 ± 0.17
SPP	1.2–1.2	3.1	1.1–1.9	0.84–0.98	2.7–4.0	0.07–0.11
CIN	3.2–3.7	7.2	2.5–4.7	-	4.9–7.4	0.19–0.27
CPI	2.2–2.5	6.1	2.7–4.9	3.1–3.3	4.5–6.2	0.25–0.33
CAPS	3.0–3.2	2.8	-	1.5–1.9	1.8–4.4	0.22–0.32
CAPS (uncorrected)	4.5–4.8	6.4	-	1.9–2.4	2.7–6.7	0.26–0.39
MODIS operational	84 ± 22	78 ± 24	27 ± 15	124 ± 28	75 ± 22	-
1.38 μm τ, operational D _e	20 ± 7.2	67 ± 27	24 ± 9.3	13 ± 3.2	66 ± 23	14
CLH	39–40	77	25–43	13–16	50–83	0.9
CSI	39–40	75	21–37	15–18	50–81	0.6
HT	27–35	75	20–36	13–16	54–93	7
MODIS operational	32 ± 4	46 ± 6	37 ± 10	22 ± 3	64 ± 11	5
CIN/CLH	37 ± 14	38 ± 9	31 ± 6	-	35 ± 6	8
CPI	37 ± 3	36 ± 2	37 ± 2	40 ± 3	42 ± 4	16
CAPS	65 ± 15	50 ± 16	-	34 ± 10	45 ± 14	25
CAPS (uncorrected)	52 ± 11	32 ± 3	-	28 ± 8	35 ± 8	19

^aFor MODIS, data are the mean ± 1σ of pixels within cloud region. For in situ τ (IWP), the values from both legs of the spiral are shown. For in situ D_e, the mean ± 1σ values are computed from the individual data points taken during both legs of the spirals.

^bFor MODIS, values are the mean of the uncertainties from each pixel within the cloud region. For the in situ IWP and τ, the values are calculated from the individual IWC and β uncertainties, and the mean uncertainty for both spiral legs (where applicable) is reported. For in situ D_e, the values are the mean of the uncertainty for D_e calculated at each point along the flight path during the spiral maneuvers.

Table 2. Statistical Comparisons of τ and IWP

	Single-Layer Data		Multilayer Data		All	
$N_{1\text{Hz}}$	2940		4080		7020	
N_{spiral}	7		4		11	
N_{MODIS}	2223		501		2724	
	Single-Layer Data Percent Difference ^a	p^b	Multilayer Data Percent Difference ^a	p^b	All Percent Difference	p^b
MODIS τ_{op} versus MODIS $\tau_{1.38}$	11.5	$<10^{-3}$	686	$<10^{-3}$	131	$<10^{-3}$
CIN versus MODIS τ_{op}	49	0.02	-59	0.02		
CPI versus MODIS τ_{op}	41	0.04	-78	0.01		
CAPS versus MODIS τ_{op}	-32	0.13	-77	0.02		
CAPS (unc) versus τ_{op}	16	0.30	-67	0.03		
CIN versus MODIS $\tau_{1.38}$					68	0.002
CPI versus MODIS $\tau_{1.38}$					48	0.002
CAPS versus MODIS $\tau_{1.38}$					1	0.34
CAPS (unc) versus $\tau_{1.38}$					53	0.03
		<i>IWP</i> (g m^{-2})				
CLH versus MODIS $IWP_{\text{op,op}}$	5	0.45	-71	0.01		
HT versus MODIS $IWP_{\text{op,op}}$	1	0.47	-75	0.01		
CSI versus MODIS $IWP_{\text{op,op}}$	-2	0.3	-71	0.01		
CLH versus MODIS $IWP_{1.38, \text{op}}$	19	0.19	55	0.07		
HT versus MODIS $IWP_{1.38, \text{op}}$	14	0.19	41	0.04		
CSI versus MODIS $IWP_{1.38, \text{op}}$	11	0.28	54	0.07		

^aFor comparison of quantity a versus b, the percent difference is $[(a - b)/b] \times 100$, where a and b are the mean values from Table 1.

^bP values are from a paired, one-sided Student's t test using the mean aircraft and satellite values from each spiral. Boldface entries are where $p \leq 0.05$, corresponding to a statistically significant difference in the mean values at the 95% significance level.

was significantly biased by the presence of low clouds. The 22 April overpass was the only other case in which low cloud cover was present. On this day, τ_{op} was a factor of ~ 4 larger than $\tau_{1.38}$, and was similarly a factor of $\sim 2-3$ larger than any of the τ from in situ measurements. For the other three overpasses with single-layered cirrus clouds (not including 6 May when the operational retrieval failed), the mean τ_{op} and $\tau_{1.38}$ agree, on average, to within 12%, which is much smaller than the 686% difference that is observed when low clouds are present. Also, as with the 30 April case discussed previously, in the 22 April case, the MODIS operational retrieval correctly identified pixels corresponding to the spiral maneuver as “multilayer ice” (not shown). In all of the single-layered cloud cases the clouds were correctly identified as being “single layer ice.” As a final piece of evidence that the operational retrieval is biased in the presence of low clouds, it is worth noting that the operational D_e was, on average, smaller than all of the in situ D_e when low clouds were present, but was larger for single-layered cirrus.

[52] On average, the mean τ_{op} (for single-layered clouds) and $\tau_{1.38}$ (in all conditions) are lower than τ calculated from the CPI, CIN, and the uncorrected CAPS data. The CAS-corrected CAPS data give a value, on average, less than the MODIS τ . However, depending on the day, the CAPS values are both above and below the MODIS τ , but are mostly within the 1σ spread of the MODIS values. It is probable that some of the disparity between in situ and MODIS τ arises from particle shattering on the in situ instruments.

[53] During MidCiX the CAS shroud was used, and number concentrations of particles larger than $100 \mu\text{m}$ ($N_{D>100}$) values were often $\sim 10 \text{ L}^{-1}$ during the spirals. These conditions were hypothesized to lead to particle shattering by *McFarquhar et al.* [2007], who estimated the CAPS extinction to be biased high by $\sim 100\%$. Such a bias in the extinction would translate directly into a bias in τ_{CAPS} of a similar amount. In this study, the τ_{CAPS} calculated using the uncorrected CAS data were on average $\sim 50\%$ larger than those using the CAS data that were

Table 3. Statistical Comparisons of D_e

	Single-layer Data		Multi layer Data		All ^a	
N_{10-s}	258		408		666	
N_{MODIS}	2108		501		2609	
	Single-layer Data Percent Difference ^b	p	Multi layer Data Percent Difference ^b	p	All ^a Percent Difference ^b	p
CIN/CLH versus MODIS operational	-26	0.10	16	-	-16	0.14
CPI versus MODIS operational	-19	0.12	49	0.16	8	0.40
CAPS versus MODIS operational	-10	0.32	79	0.14	34	0.27
CAPS (unc) versus MODIS operational	-38	0.11	45	0.16	4	0.36

^aP values are from a one-sided, paired, Student's t test. Results from these tests are not statistically significant, in part, because of the small number of data points (i.e., $N_{\text{single-layer}} = 3$, $N_{\text{multi-layer}} = 2$, and $N_{\text{all}} = 5$).

^bFor comparison of quantity a versus b, the percent difference is $[(a - b)/b] \times 100$, where a and b are the mean values from Table 1.

corrected for shattering. Also, the uncorrected τ_{CAPS} were $\sim 50\%$ larger than the $\tau_{1.38}$ values on average, and 16% larger than τ_{op} for single-layer clouds. Overall, these results support the claim by McFarquhar et al. that particle shattering biases the CAS measurements, but the magnitude of the effect observed in this study is not as large. There are a number of reasons that this effect may be smaller, including limitations of the comparison method, MODIS retrieval biases, a smaller shattering effect than that claimed by McFarquhar et al., or some combination of the above. Nevertheless, reducing the uncorrected τ_{CAPS} by a factor of two, as implied by McFarquhar et al., would result in values that are systematically lower than those from MODIS.

[54] Besides particle shattering, biases in the MODIS retrievals due to subpixel heterogeneity of the cloud field and 3D radiative effects cannot be ruled out as an explanation for differences between the MODIS and aircraft values of optical depth. Several studies have addressed the issue of how these effects have the potential to produce both uncertainty and bias in the MODIS τ/τ_e retrievals, although these studies have focused on low-altitude liquid clouds, and not cirrus [e.g., *Iwabuchi and Hayasaka*, 2002; *Kato et al.*, 2006; *Marshak et al.*, 2006; *Varnai and Marshak*, 2001].

[55] For the IWP data, many features are similar to those seen in the τ data with regard to single-layered and multilayered clouds. The $\text{IWP}_{\text{op,op}}$ is significantly larger than the IWP calculated from in situ observations for the two low-cloud cover cases on 22 April and 30 April. For the single-layer cloud cases, both $\text{IWP}_{\text{op,op}}$ and $\text{IWP}_{1.38,\text{op}}$ values agree with the in situ IWP to within 20% on average.

[56] Also included in Figure 6 are median IWPs (i.e., $\langle \text{IWP}_{1.38,\langle x \rangle} \rangle$) calculated using $\tau_{1.38}$ and the median values of the in situ D_e (plotted as pluses). The resulting ranges of values are an indicator of how sensitive the MODIS-based IWPs are to the assumed D_e , using the different values of in situ D_e as a proxy for the uncertainty in this quantity. For most of the overpasses, the spread of in situ D_e leads to a spread of $\langle \text{IWP}_{1.38,\langle x \rangle} \rangle$ that is larger than the standard deviation of $\text{IWP}_{1.38,\text{op}}$ (i.e., $\pm 1\sigma$ bars). That is to say, the range of in situ D_e cause a larger spread in the MODIS-based IWP than the inherent horizontal heterogeneity of IWP at the spatial scale of MODIS. Ideally, the range of $\text{IWP}_{1.38,\langle x \rangle}$ would lie well within the span of in situ IWP measurements, and would be smaller than the variability in $\text{IWP}_{1.38,\text{op}}$.

5. Conclusions

[57] In this paper, data from the MidCiX field campaign obtained in coincidence with Terra and Aqua overpasses were compared with an offline MODIS cirrus retrieval from the 1.38- μm channel, as well as the MODIS operational cloud product. The MidCiX data set provided a unique opportunity for direct comparison of airborne in situ measurements with satellite retrievals. These comparisons were used to assess the quality of both the aircraft and satellite measurements, and to investigate the fundamental limits of these types of direct aircraft/satellite comparisons.

[58] Several important conclusions can be drawn from the MidCiX comparisons presented here. First, it is clear that

the uncertainties and potential biases in the aircraft-borne β/D_e measurements, as manifested by the spread of values, are too large to provide any stringent constraint on satellite-retrieved quantities. In general, τ calculated from the uncorrected CAPS data were the highest during MidCiX, with CPI, CAPS, and CIN in the middle, and SPP on the low end. This general pattern is not surprising. The SPP measures particles with diameters between about 1 and 50 μm , and thus misses some contribution to the extinction from larger particles. On the other end of the extinction spectrum, the high (uncorrected) τ_{CAPS} values are not surprising given the presence of the CAS shroud during MidCiX and the previously identified problems associated with particle shattering on the shroud [*McFarquhar et al.*, 2007]. Qualitatively, the corrected τ_{CAPS} are in much better agreement with both the MODIS and other in situ τ , although a detailed evaluation of the CAS correction is beyond the scope of this work.

[59] These τ comparisons are different than similar observations made during CRYSTAL-FACE, where CIN measured extinctions larger by a factor of ~ 2 than those calculated from the size distributions measured by particle instruments [*Heymsfield et al.*, 2006]. The reason that CIN extinctions were significantly larger than the particle-probe extinctions during CRYSTAL-FACE, but not during Mid-CiX, is not well understood. It is possible that the differences are related to instrument location, data processing method, and/or data quality assurance.

[60] Given all of these caveats, however, it is clear that during MidCiX the values of τ calculated from the uncorrected CAPS, CPI, and CIN measurements were systematically larger than those from the MODIS retrievals (excluding τ_{op} bias from multilayer clouds). This behavior is consistent with an overestimation of extinction by the particle probes due to particle shattering on inlet surfaces. However, definitively ascribing the differences to shattering is not possible, as biases in the MODIS retrievals cannot be ruled out, and issues such as cloud heterogeneity may affect in a fundamental way the comparison between satellite and aircraft data.

[61] Although not statistically significant, the in situ D_e were, on average, smaller than the MODIS values for single-layer cloud cases, as would be expected if particle shattering were occurring. Similarly, for multilayered cloud cases, the MODIS D_e were smaller than the in situ D_e , which is qualitatively consistent with a bias due to a low liquid-cloud layer containing droplets that are smaller than those in the upper cirrus layer. With respect to the individual instruments, the CAPS D_e were closest to the MODIS values in an average sense, but with large scatter, whereas the CPI D_e showed little variability and were consistently 40–50 μm . The D_e calculated from the CIN β and CLH IWC (or any other bulk IWC) were smaller, on average, than the MODIS values in single-layered clouds, although the differences were not as large as would be expected (i.e., CIN D_e a factor of 2 or more low relative to MODIS) from previous studies [*Heymsfield et al.*, 2006] if MODIS values are taken as “truth.”

[62] In contrast to the extinction and effective size measurements, the in situ IWC measurements are in good agreement with one another, and there is greater confidence in their accuracy [*Davis et al.*, 2007a]. For single-layered

cloud cases, the in situ IWP were in agreement (to within 1σ) with both the MODIS operational IWP values and IWP calculated using the MODIS $1.38\text{-}\mu\text{m}$ τ and operational D_e . For the low cloud cover cases, the operational IWP were upward of an order of magnitude larger than the in situ IWP, whereas the $1.38\text{-}\mu\text{m}$ IWP were in better agreement with the in situ data. The agreement in single-layer cloud cases is somewhat surprising, given that the (relative) uncertainties in the MODIS IWP values are higher than for τ or D_e individually, since IWP is a product of the two (e.g., see equation (7)), and there is a covariance term in the IWP error estimate.

[63] Despite the incomplete agreement between the MODIS and in situ data, this study has illustrated an important limitation of the MODIS operational retrieval: it overestimates the cirrus cloud optical thickness for scenes in which a cirrus layer overlaps a lower cloud layer. This limitation has been anticipated on the basis of the expected effect of multilayered cloud systems on the top of atmosphere radiances [Chang and Li, 2005b], but the MidCiX data provide direct evidence that the operationally retrieved cirrus optical properties can be skewed by more than an order of magnitude by the presence of low cloud layers. Agreement between τ_{op} and $\tau_{1.38}$ in single layer cirrus scenes over both land and ocean support the hypothesis that differences between these retrievals are due to lower cloud layer contamination in the operational retrieval, and not land surface effects. Further research, perhaps using the multilayer cloud flag and data from the CloudSat radar or CALIPSO lidar on the A-Train [Stephens et al., 2002], is needed to better understand differences between the operational and $1.38\text{-}\mu\text{m}$ retrieval in the presence of overlapped clouds.

[64] The limitations of the operational MODIS optical thickness retrieval in multilayered cloud scenes may have implications for attempts to quantify the relationship between cirrus optical properties and radiative forcing. For example, Choi and Ho [2006] used gridded optical properties (MOD08) from the MOD06 product with the Clouds and the Earth's Radiant Energy System (CERES) [Wielicki et al., 1996] longwave (LW) and shortwave (SW) fluxes to evaluate the net cloud radiative effect (CRE, W m^{-2}) of cirrus as a function of optical thickness. They find, similar to other studies, that CRE is positive with increasing optical thickness up to a threshold, beyond which it is negative. The threshold is found to occur at $\tau = 10$, independent of season or location. This result is in contrast to the same authors' previous work, which gave a threshold value of $\tau = 3$ based on a radiative transfer model [Choi et al., 2005], and is also different from the cirrus parameterization of Fu and Liou [1993], which has a threshold of $\tau = 6.5$ (for clouds with $D_e = 25 \mu\text{m}$). One major difference between the data considered by Choi and Ho versus that used in other research is that the former presumably contains both single-layer cirrus and cirrus overlapping low clouds, whereas previous radiative transfer model-based estimates of CRE versus τ were only applicable to single-layer cirrus. The presence of a high bias in the MOD08 optical thicknesses from multilayered clouds offers one explanation for the discrepancy between the τ threshold value from Choi and Ho and previous work.

[65] Finally, the comparisons in this paper highlight some of the fundamental challenges to direct comparison of

satellite and aircraft data in cirrus clouds. Because of the dynamic nature of cirrus clouds, it was found that any time lag between the aircraft and satellite data necessitated an "advection" of the aircraft flight track in order to match the spatial locations of the aircraft and satellite data. This advection accounts for cloud movement between the time of the aircraft and satellite sampling, but does not account for growth or decay of cirrus in the intervening time period. For all of the cases considered in this paper, the lags between aircraft and satellite times were less than one hour. No obvious trends exist in the difference between the satellite and aircraft data as a function of lag time (not shown), but the lack of trend may be due to the small sample size and the large spread in the measurements. In order to minimize the effects of cloud evolution and advection uncertainties, it is still important to minimize the time lag between aircraft and satellite sampling in planning for these types of direct comparisons. Also, it is desirable for the aircraft to sample after the satellite overpass in order to eliminate the potential for contrail contamination of the scene, especially for comparisons in thin cirrus where the optical thicknesses are of similar magnitude to contrails.

[66] It was also found that the horizontal heterogeneity of the τ and IWP fields viewed at the MODIS resolution of 1 km, as manifested in the spread of the τ or IWP histograms, provides a useful benchmark for the required accuracy of in situ data necessary to provide a meaningful constraint on remotely sensed quantities. In other words, the in situ data from different instruments would ideally agree within the spread of satellite-retrieved values of τ and IWP. When this is the case, the comparison between aircraft and satellite data can be interpreted with increased confidence that the agreement is significant and not spurious. As of now, this level of agreement does not exist among the in situ measurements of β or τ , but does for the in situ IWC/IWP measurements. The experimental community is actively addressing the disparity among the in situ extinction measurements, and the results discussed here highlight the need for this issue to be resolved.

[67] **Acknowledgments.** The authors would like to thank those involved in the planning and execution of the MidCiX mission, in particular Jay Mace, the MidCiX flight planning team, and the WB-57F flight and ground crews. We also thank the instrument PIs for their work in obtaining and providing data, including Elliot Weinstock, Cynthia Twohy, Tim Garrett, and Paul Lawson. Funding for participation in the MidCiX campaign and subsequent data analysis was provided to L.M.A. by the NASA Radiation Sciences Program, under the direction of Don Anderson and Hal Maring. S.M.D. recognizes the support of the NASA ESS Fellowship program, and numerous helpful discussions with Tim Garrett, Andy Heymsfield, Paul Lawson, Steve Platnick, and Eric Jensen. B.H.K. was funded by the NASA Post-doctoral Program during this study and acknowledges the support of the NASA Radiation Sciences Program directed by Hal Maring. K.G.M. was partly supported by a NASA grant (NNG05GL78G) and a NASA Earth System Science Fellowship (NNG04GQ92H). MODIS operational data were downloaded from <http://ladsweb.nascom.nasa.gov/>.

References

- Baker, B., and R. P. Lawson (2006), Improvement in determination of ice water content from two-dimensional particle imagery. Part I: Image-to-mass relationships, *J. Appl. Meteorol. Climatol.*, 45(9), 1282–1290, doi:10.1175/JAM2398.1.
- Baumgardner, D., H. Jonsson, W. Dawson, D. O'Connor, and R. Newton (2001), The cloud, aerosol and precipitation spectrometer: A new instrument

- for cloud investigations, *Atmos. Res.*, 59–60, 251–264, doi:10.1016/S0169-8095(01)00119-3.
- Chang, F. L., and Z. Q. Li (2005a), A near-global climatology of single-layer and overlapped clouds and their optical properties retrieved from Terra/MODIS data using a new algorithm, *J. Clim.*, 18(22), 4752–4771, doi:10.1175/JCLI3553.1.
- Chang, F. L., and Z. Q. Li (2005b), A new method for detection of cirrus overlapping water clouds and determination of their optical properties, *J. Atmos. Sci.*, 62(11), 3993–4009, doi:10.1175/JAS3578.1.
- Chepfer, H., G. Brogniez, P. Goloub, F. M. Breon, and P. H. Flamant (1999), Observations of horizontally oriented ice crystals in cirrus clouds with POLDER-1/ADEOS-1, *J. Quant. Spectrosc. Radiat. Transfer*, 63(2–6), 521–543.
- Chiriaco, M., et al. (2007), Comparison of CALIPSO-like, LaRC, and MODIS retrievals of ice-cloud properties over SIRTa in France and Florida during CRYSTAL-FACE, *J. Appl. Meteorol. Climatol.*, 46(3), 249–272, doi:10.1175/JAM2435.1.
- Choi, Y. S., and C. H. Ho (2006), Radiative effect of cirrus with different optical properties over the tropics in MODIS and CERES observations, *Geophys. Res. Lett.*, 33, L21811, doi:10.1029/2006GL027403.
- Choi, Y. S., C. H. Ho, and C. H. Sui (2005), Different optical properties of high cloud in GMS and MODIS observations, *Geophys. Res. Lett.*, 32, L23823, doi:10.1029/2005GL024616.
- Davis, S. M., L. M. Avallone, E. M. Weinstock, C. H. Twohy, J. B. Smith, and G. L. Kok (2007a), Comparisons of in situ measurements of cirrus cloud ice water content, *J. Geophys. Res.*, 112, D10212, doi:10.1029/2006JD008214.
- Davis, S. M., A. G. Hallar, L. M. Avallone, and W. Engblom (2007b), Measurement of total water with a tunable diode laser hygrometer: Inlet analysis, calibration procedure, and ice water content determination, *J. Atmos. Oceanic Technol.*, 24(3), 463–475, doi:10.1175/JTECH1975.1.
- Dessler, A. E., and P. Yang (2003), The distribution of tropical thin cirrus clouds inferred from Terra MODIS data, *J. Clim.*, 16(8), 1241–1247, doi:10.1175/1520-0442(2003)16<1241:TDOTTC>2.0.CO;2.
- Elouragini, S., H. Chtioui, and P. H. Flamant (2005), Lidar remote sounding of cirrus clouds and comparison of simulated fluxes with surface and METEOSAT observations, *Atmos. Res.*, 73, 23–36, doi:10.1016/j.atmosres.2004.07.003.
- Fu, Q., and K. N. Liou (1993), Parameterization of the radiative properties of cirrus clouds, *J. Atmos. Sci.*, 50(13), 2008–2025, doi:10.1175/1520-0469(1993)050<2008:POTRPO>2.0.CO;2.
- Gao, B. C., and Y. J. Kaufman (1995), Selection of the 1.375- μm MODIS channel for remote sensing of cirrus clouds and stratospheric aerosols from space, *J. Atmos. Sci.*, 52(23), 4231–4237, doi:10.1175/1520-0469(1995)052<4231:SOTMCF>2.0.CO;2.
- Garrett, T. J. (2007), Comment on “Effective radius of ice cloud particle populations derived from aircraft probes,” *J. Atmos. Oceanic Technol.*, 24(8), 1495–1502, doi:10.1175/JTECH2075.1.
- Gerber, H. (2007), Comment on “Effective radius of ice cloud particle populations derived from aircraft probes,” *J. Atmos. Oceanic Technol.*, 24(8), 1504–1510, doi:10.1175/JTECH2076.1.
- Gerber, H., Y. Takano, T. J. Garrett, and P. V. Hobbs (2000), Nephelometer measurements of the asymmetry parameter, volume extinction coefficient, and backscatter ratio in Arctic clouds, *J. Atmos. Sci.*, 57(18), 3021–3034, doi:10.1175/1520-0469(2000)057<3021:NMOTAP>2.0.CO;2.
- Hawkinson, J. A., W. Feltz, and S. A. Ackerman (2005), A comparison of GOES sounder- and cloud lidar- and radar-retrieved cloud-top heights, *J. Appl. Meteorol.*, 44(8), 1234–1242, doi:10.1175/JAM2269.1.
- Heymsfield, A. J., C. Schmitt, A. Bansemmer, G. J. van Zadelhoff, M. R. J. McGill, C. Twohy, and D. Baumgardner (2006), Effective radius of ice cloud particle populations derived from aircraft probes, *J. Atmos. Oceanic Technol.*, 23(3), 361–380, doi:10.1175/JTECH1857.1.
- Hollars, S., Q. A. Fu, J. Comstock, and T. Ackerman (2004), Comparison of cloud-top height retrievals from ground-based 35 GHz MMCR and GMS-5 satellite observations at ARM TWP Manus site, *Atmos. Res.*, 72, 169–186, doi:10.1016/j.atmosres.2004.03.015.
- Iwabuchi, H., and T. Hayasaka (2002), Effects of cloud horizontal inhomogeneity on the optical thickness retrieved from moderate-resolution satellite data, *J. Atmos. Sci.*, 59(14), 2227–2242, doi:10.1175/1520-0469(2002)059<2227:EOCHIO>2.0.CO;2.
- Kahn, B. H., A. Eldering, A. J. Braverman, E. J. Fetzer, J. H. Jiang, E. Fishbein, and D. L. Wu (2007), Toward the characterization of upper tropospheric clouds using Atmospheric Infrared Sounder and Microwave Limb Sounder observations, *J. Geophys. Res.*, 112, D05202, doi:10.1029/2006JD007336.
- Kato, S., L. M. Hinkelman, and A. N. Cheng (2006), Estimate of satellite-derived cloud optical thickness and effective radius errors and their effect on computed domain-averaged irradiances, *J. Geophys. Res.*, 111, D17201, doi:10.1029/2005JD006668.
- King, M. D., S.-C. Tsay, S. E. Platnick, M. Wang, and K. N. Liou (1997), Cloud retrieval algorithms for MODIS: Optical thickness, effective particle radius, and thermodynamic phase, *ATBD-MOD-05*, 79 pp., NASA Goddard Space Flight Center, Greenbelt, Md.
- Lawson, R. P., B. A. Baker, C. G. Schmitt, and T. L. Jensen (2001), An overview of microphysical properties of Arctic clouds observed in May and July 1998 during FIRE ACE, *J. Geophys. Res.*, 106(D14), 14,989–15,014, doi:10.1029/2000JD900789.
- Mace, G. G., Y. Y. Zhang, S. Platnick, M. D. King, P. Minnis, and P. Yang (2005), Evaluation of cirrus cloud properties derived from MODIS data using cloud properties derived from ground-based observations collected at the ARM SGP site, *J. Appl. Meteorol.*, 44(2), 221–240, doi:10.1175/JAM2193.1.
- Mahesh, A., M. A. Gray, S. P. Palm, W. D. Hart, and J. D. Spinhirne (2004), Passive and active detection of clouds: Comparisons between MODIS and GLAS observations, *Geophys. Res. Lett.*, 31, L04108, doi:10.1029/2003GL018859.
- Marshak, A., S. Platnick, T. Varnai, G. Y. Wen, and R. F. Cahalan (2006), Impact of three-dimensional radiative effects on satellite retrievals of cloud droplet sizes, *J. Geophys. Res.*, 111, D09207, doi:10.1029/2005JD006686.
- McFarquhar, G. M., J. Um, M. Freer, D. Baumgardner, G. L. Kok, and G. Mace (2007), Importance of small ice crystals to cirrus properties: Observations from the Tropical Warm Pool International Cloud Experiment (TWP-ICE), *Geophys. Res. Lett.*, 34, L13803, doi:10.1029/2007GL029865.
- Meyer, K., P. Yang, and B. C. Gao (2007), Ice cloud optical depth from MODIS cirrus reflectance, *IEEE Trans. Geosci. Remote Sens.*, 45(3), 471–474, doi:10.1109/LGRS.2007.897428.
- Minnis, P., J. K. Ayers, R. Palikonda, and D. Phan (2004), Contrails, cirrus trends, and climate, *J. Clim.*, 17(8), 1671–1685, doi:10.1175/1520-0442(2004)017<1671:CCTAC>2.0.CO;2.
- Mitchell, D. L. (2002), Effective diameter in radiation transfer: General definition, applications, and limitations, *J. Atmos. Sci.*, 59(15), 2330–2346, doi:10.1175/1520-0469(2002)059<2330:EDIRTG>2.0.CO;2.
- Nakajima, T., and M. D. King (1990), Determination of the optical-thickness and effective particle radius of clouds from reflected solar-radiation measurements. 1. Theory, *J. Atmos. Sci.*, 47(15), 1878–1893, doi:10.1175/1520-0469(1990)047<1878:DOTOTA>2.0.CO;2.
- Nasiri, S. L., and B. H. Kahn (2008), Limitations of bi-spectral infrared cloud phase determination and potential for improvement, *J. Appl. Meteorol. Climatol.*, 47(11), 2895–2910, doi:10.1175/2008JAMC1879.1.
- Naud, C., J. P. Muller, and E. E. Clothiaux (2002), Comparison of cloud top heights derived from MISR stereo and MODIS CO₂-slicing, *Geophys. Res. Lett.*, 29(16), 1795, doi:10.1029/2002GL015460.
- Naud, C., J. P. Muller, M. Haeffelin, Y. Morille, and A. Delaval (2004), Assessment of MISR and MODIS cloud top heights through intercomparison with a back-scattering lidar at SIRTa, *Geophys. Res. Lett.*, 31, L04114, doi:10.1029/2003GL018976.
- Naud, C. M., B. A. Baum, M. Pavolonis, A. Heidinger, R. Frey, and H. Zhang (2007), Comparison of MISR and MODIS cloud-top heights in the presence of cloud overlap, *Remote Sens. Environ.*, 107(1–2), 200–210, doi:10.1016/j.rse.2006.09.030.
- Platnick, S. (2000), Vertical photon transport in cloud remote sensing problems, *J. Geophys. Res.*, 105(D18), 22,919–22,935.
- Platnick, S., M. D. King, S. A. Ackerman, W. P. Menzel, B. A. Baum, J. C. Riedi, and R. A. Frey (2003), The MODIS cloud products: Algorithms and examples from Terra, *IEEE Trans. Geosci. Remote Sens.*, 41(2), 459–473, doi:10.1109/TGRS.2002.808301.
- Rolland, P., K. N. Liou, M. D. King, S. C. Tsay, and G. M. McFarquhar (2000), Remote sensing of optical and microphysical properties of cirrus clouds using Moderate-Resolution Imaging Spectroradiometer channels: Methodology and sensitivity to physical assumptions, *J. Geophys. Res.*, 105(D9), 11,721–11,738, doi:10.1029/2000JD900028.
- Scott, S. G., T. P. Bui, K. R. Chan, and S. W. Bowen (1990), The meteorological measurement system on the NASA Er-2 aircraft, *J. Atmos. Oceanic Technol.*, 7(4), 525–540, doi:10.1175/1520-0426(1990)007<0525:TMMSOT>2.0.CO;2.
- Sherwood, S. C., J. H. Chae, P. Minnis, and M. McGill (2004), Underestimation of deep convective cloud tops by thermal imagery, *Geophys. Res. Lett.*, 31, L11102, doi:10.1029/2004GL019699.
- Smith, W. L., and C. M. R. Platt (1978), Comparison of satellite-deduced cloud heights with indications from radiosonde and ground-based laser measurements, *J. Appl. Meteorol.*, 17(12), 1796–1802, doi:10.1175/1520-0450(1978)017<1796:COCDCH>2.0.CO;2.
- Stephens, G. L., et al. (2002), The CloudSat mission and the A-Train—A new dimension of space-based observations of clouds and precipitation, *Bull. Am. Meteorol. Soc.*, 83(12), 1771–1790, doi:10.1175/BAMS-83-12-1771.
- Stubenrauch, C. J., F. Eddouia, and L. Sauvage (2005), Cloud heights from TOVS Path-B: Evaluation using LITE observations and distributions of highest cloud layers, *J. Geophys. Res.*, 110, D19203, doi:10.1029/2004JD005447.

- Tian, L., and J. A. Curry (1989), Cloud overlap statistics, *J. Geophys. Res.*, *94*(D7), 9925–9935, doi:10.1029/JD094iD07p09925.
- Twohy, C. H., A. J. Schanot, and W. A. Cooper (1997), Measurement of condensed water content in liquid and ice clouds using an airborne counterflow virtual impactor, *J. Atmos. Oceanic Technol.*, *14*(1), 197–202, doi:10.1175/1520-0426(1997)014<0197:MOCWCI>2.0.CO;2.
- Vanbauce, C., B. Cadet, and R. T. Marchand (2003), Comparison of POLDER apparent and corrected oxygen pressure to ARM/MMCR cloud boundary pressures, *Geophys. Res. Lett.*, *30*(5), 1212, doi:10.1029/2002GL016449.
- Varnai, T., and A. Marshak (2001), Statistical analysis of the uncertainties in cloud optical depth retrievals caused by three-dimensional radiative effects, *J. Atmos. Sci.*, *58*(12), 1540–1548, doi:10.1175/1520-0469(2001)058<1540:SAOTUI>2.0.CO;2.
- Wang, L. K., and A. E. Dessler (2006), Instantaneous cloud overlap statistics in the tropical area revealed by ICESat/GLAS data, *Geophys. Res. Lett.*, *33*, L15804, doi:10.1029/2005GL024350.
- Warren, S. G., C. J. Hahn, and J. London (1985), Simultaneous occurrence of different cloud types, *J. Clim. Appl. Meteorol.*, *24*(7), 658–667, doi:10.1175/1520-0450(1985)024<0658:SODCT>2.0.CO;2.
- Weinstock, E. M., et al. (2006a), Measurements of the total water content of cirrus clouds, Part I: Instrument details and calibration, *J. Atmos. Oceanic Technol.*, *23*(11), 1397–1409.
- Weinstock, E. M., J. B. Smith, D. Sayres, J. V. Pittman, N. Allen, and J. G. Anderson (2006b), Measurements of the total water content of cirrus clouds, Part II: Instrument performance and validation, *J. Atmos. Oceanic Technol.*, *23*(11), 1410–1421.
- Wielicki, B. A., J. T. Suttles, A. J. Heymsfield, R. M. Welch, J. D. Spinhirne, M. L. C. Wu, D. O. Starr, L. Parker, and R. F. Arduini (1990), The 27–28 October 1986 FIRF IFO cirrus case study: Comparison of radiative-transfer theory with observations by satellite and aircraft, *Mon. Weather Rev.*, *118*(11), 2356–2376, doi:10.1175/1520-0493(1990)118<2356:TOFICC>2.0.CO;2.
- Wielicki, B. A., B. R. Barkstrom, E. F. Harrison, R. B. Lee, G. L. Smith, and J. E. Cooper (1996), Clouds and the Earth's radiant energy system (CERES): An Earth observing system experiment, *Bull. Am. Meteorol. Soc.*, *77*(5), 853–868, doi:10.1175/1520-0477(1996)077<0853:CATERE>2.0.CO;2.
- Wylie, D. P., and P. H. Wang (1999), Comparison of SAGE-II and HIRS co-located cloud height measurements, *Geophys. Res. Lett.*, *26*(22), 3373–3375, doi:10.1029/1999GL010857.
- Yue, Q., K. N. Liou, S. C. Ou, B. H. Kahn, P. Yang, and G. G. Mace (2007), Interpretation of AIRS data in thin cirrus atmospheres based on a fast radiative transfer model, *J. Atmos. Sci.*, *64*(11), 3827–3842, doi:10.1175/2007JAS2043.1.
-
- L. M. Avallone, Laboratory for Atmospheric and Space Physics, University of Colorado, 1234 Innovation Drive, Boulder, CO 80303, USA. (linnea.avallone@lasp.colorado.edu)
- D. Baumgardner, Centro de Ciencias de la Atmósfera, Universidad Nacional Autónoma de México, 04510 Mexico City, Mexico. (darrel@servidor.unam.mx)
- S. M. Davis, Cooperative Institute for Research in Environmental Sciences, University of Colorado, 216 UCB, Boulder, CO 80309-0216, USA. (seand@colorado.edu)
- B. H. Kahn, Jet Propulsion Laboratory, Mail Stop 169-237, 4800 Oak Grove Drive, Pasadena, CA 91109, USA. (brian.h.kahn@jpl.nasa.gov)
- K. G. Meyer, NASA Goddard Space Flight Center, Mailstop 613.2, Greenbelt, MD 20771, USA. (Kerry.G.Meyer@nasa.gov)